THE JOURNAL OF PHYSICAL CHEMISTRY C

Article

pubs.acs.org/JPCC

A Combined Experimental–Computational Investigation of Methane Adsorption and Selectivity in a Series of Isoreticular Zeolitic Imidazolate Frameworks

Yao Houndonougbo,*[,†] Christopher Signer,[†] Ning He,[‡] William Morris,[§] Hiroyasu Furukawa,[§] Keith G. Ray,[∥] David L. Olmsted,[⊥] Mark Asta,[⊥] Brian B. Laird,[‡] and Omar M. Yaghi[#]

[†]Department of Chemistry and Biochemistry, Eastern Washington University, Cheney, Washington 99004, United States

[‡]Department of Chemistry, University of Kansas, Lawrence, Kansas 66045, United States

[§]Department of Chemistry and Biochemistry, University of California, Los Angeles, California 90095, United States

Departments of [∥]Physics, [⊥]Materials Science and Engineering, and [#]Chemistry, University of California, Berkeley, California 94720, United States

Supporting Information

ABSTRACT: Zeolitic imidazolate framework (ZIF) materials have received considerable attention recently due to their potential as materials for gas separation applications. In this work, we study, both experimentally and with molecular modeling, methane adsorption in a series of five ZIFs (ZIF-25, -71, -93, -96, and -97) that share a common structural topology (RHO), but differ in imidazolate functionalization. Such a series allows for the direct assessment of the role that functionalization plays in determining methane adsorption. Experimental measurements of methane adsorption up to 1 bar at various temperatures are well reproduced by molecular simulations, which are further used to examine adsorption up to higher pressures of 80 bar, and to analyze the preferred binding sites within the structure. We find that CH_4 uptake in these ZIFs is roughly proportional to the Brunauer–Emmett–Teller (BET) surface area, in contrast to our earlier work on the adsorption of CO_2 for this series [*J. Am. Chem. Soc.* **2010**, *132*, 11006], which showed a significant enhancement of CO_2 adsorption, due to electrostatic effects, in asymmetrically functionalized ZIFs (ZIF-93, -96, -97) over those with symmetric functionalization (ZIF-25, -71). Furthermore, the ideal adsorbed solution theory (IAST) is used to predict selectivity of CO_2 over CH_4 in these RHO ZIFs by fitting CH_4 adsorption measurements in this work and the CO_2 experimental isotherms from our earlier work [*J. Am. Chem. Soc.* **2010**, *132*, 11006].

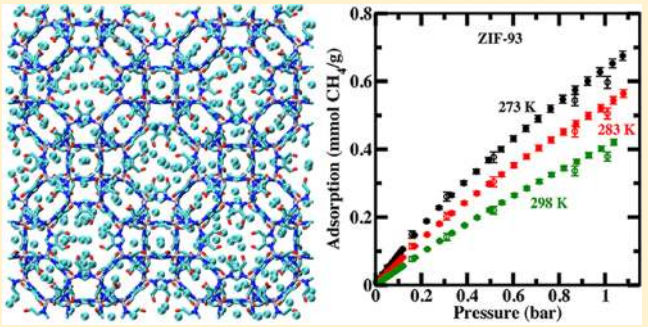

INTRODUCTION

Methane (CH_4) is the major component of natural gas, which is considered a cleaner energy source relative to other fossil fuels because of its higher hydrogen-to-carbon ratio and lower carbon emission. However, the energy content of natural gas is reduced by the presence of carbon dioxide (CO_2) as one of the main impurities.[1] The common industrial methods used for CO_2 separations from gas mixtures rely on solvent absorption, cryogenic separations, membrane separations, or adsorption by solid sorbents.[2] Separation by solid–sorbent adsorption, as compared to other methods, offers potential advantages such as reduced environmental impact and mild pressure and temperature operating conditions.[1,3,4]

Recently, metal–organic frameworks (MOFs) have emerged as a new class of materials that have great potential for use in gas capture and separation applications.[5−10] MOFs are highly crystalline, nanoporous materials with a building-block formed by metal atoms linked by coordinating organic bridging ligands. They have attracted much attention because of their high porosity, very high surface area, and potential for tailoring pore sizes and chemical environment to particular properties.[7,11,12] Zeolitic imidazole frameworks (ZIFs) are a subclass of MOFs that have received significant attention very recently because of their high porosity, their thermal and chemical stability, and their enormous variability with respect to topology and functionality.[13−16] ZIFs, which are composed of tetrahedrally coordinated metal centers such as Zn and Co linked by functionalized imidazole groups, are being actively investigated for membrane-based gas separations relevant to natural gas applications, either as pure membrane materials or as a component in polymer-composite membranes.[17−26]

Received: September 27, 2012
Revised: April 6, 2013
Published: April 10, 2013

In this work, we examine, using both experiment and molecular modeling, methane adsorption and selectivity (relative to CO_2) in a previously reported[27] series of ZIFs: ZIF-25, -71, -93, -96, and -97. This ZIF series is isoreticular; that is, the materials in the series share the same topology, in this case RHO, but differ by linker functionalization, as illustrated in Figure 1. This series is, to our knowledge, the

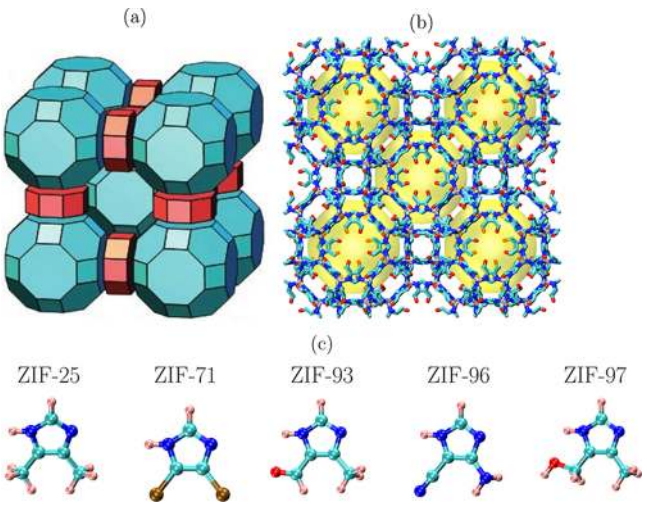

Figure 1. (a) Polyhedral packing of the RHO structure (blue and red polyhedral represent the subdivisions of space). (b) Structures of the RHO topology ZIFs in ZIF-93. The free space within the α-cavities is represented by a yellow sphere. Hydrogen atoms are omitted for clarity. (c) Representations of the Imidazolate-type linkers in the ZIFs. Atom colors in (a,b): zinc, silver; carbon, cyan; nitrogen, blue; oxygen, red; hydrogen, pink; chlorine, ochre.

largest isoreticular series of ZIF materials to be studied with uniform experimental and computational techniques to date, which allows us to study directly the effect of functionalization on adsorption. Many previous investigations of CH_4 adsorption and selectivity in ZIFs[16,28−37] involve either studies of single ZIFs or comparisons between nonisoreticular ZIF materials, making it difficult to assess the role of functionalization and topology independently. There have been a few similar studies of methane adsorption and selectivity in other isoreticular ZIF sets, but these were focused either on GME[15,24,38−41] or SOD[41−43] topologies.

For the RHO ZIFs considered in the present work, low-pressure methane uptake was measured at 298 K, 283 K, and 273 K. The measurements are complemented by molecular simulations, which are used to investigate adsorption isotherms up to 80 bar, and to investigate dominant binding sites. Isosteric heats of adsorption are derived as functions of loading from both experiment and simulation. Finally, the results of the present study are combined with previous data for CO_2 adsorption in the same ZIF materials[27] to determine adsorption selectivity from ideal adsorbed solution theory (IAST) calculations at low pressures.

METHODOLOGY

Experimental Methods. The isoreticular series of ZIFs was synthesized and activated from reported preparations.[27] Low pressure gas adsorption isotherms were measured volumetrically on an Autosorb-1 analyzer (Quantachrome Instruments). A constant temperature water bath at (273, 283, 298 K) was used for CH_4 measurements. The CH_4 gas used was ultrahigh purity (UHP) grade. Estimated error of these measurements is ±2%.

Classical Force Fields for Simulations. The intermolecular interactions of all molecules studied in this work are represented by pairwise-additive Lennard−Jones (LJ) 12-6 potentials

$$U(r_{ij}) = 4\varepsilon_{ij}\left[\left(\frac{\sigma_{ij}}{r_{ij}}\right)^{12} - \left(\frac{\sigma_{ij}}{r_{ij}}\right)^{6}\right] \quad (1)$$

where r_{ij}, ε_{ij}, and σ_{ij} are the separation, LJ well depth, and LJ size, respectively, for interacting atoms i and j. The cross-interaction parameters ε_{ij} and σ_{ij} were calculated using Lorentz−Berthelot mixing rules.[44] Molecular simulation studies have shown that LJ parameters of generic force fields such as UFF and OPLS-AA can accurately predict adsorption in ZIFs.[27,45−47] Although these force fields perform well in some ZIFs, their transferability and ability to describe the short-range vdW interactions in ZIFs is limited.[27,31] A number of efforts have been made to develop transferable force fields from ab initio calculations for H_2[48] and CO_2 adsorption in ZIFs;[49−51] however, such ab-initio-based transferable force fields for CH_4 are not, to our knowledge, available in the literature.

In this work, we model the methane molecule using the Transferable Potentials for Phase Equilibria United Atom (TraPPE-UA) force field,[52] in which CH_4 is modeled as a single, uncharged LJ sphere located on the carbon atom. For the ZIF atoms, we use LJ parameters taken from the Optimized Potentials for Liquid Simulations All Atom (OPLS-AA) force field.[53,54] As there are no OPLS-AA parameters for Zn, these are taken from the Universal Force Field (UFF).[55] All the Lennard−Jones parameters are listed in Table 2.

Molecular Simulation. The initial structures of the ZIFs were constructed from the atomic coordinates given in our previous work.[27] The 2 × 2 × 1 unit cells of the ZIFs used in the simulations are shown in Figure 1a. The periodic building unit of the RHO topology ZIFs consists of an α-cavity (also sometimes referred to as an LTA cavity) that is composed of 12 four-membered rings, 8 six-membered rings, and 6 eight-membered rings. The α-cavities are connected through double eight-membered rings in a body-centered cubic arrangement as shown in Figure 1. To determine the isotherms and adsorption thermodynamics, we employ grand canonical Monte Carlo simulations implemented using the Monte Carlo for Complex Chemical Systems (MCCCS) Towhee program.[56] The non-bonded Lennard−Jones interactions were truncated at 13 Å, and standard long-range corrections were employed.[57] The ZIFs used in the simulations were modeled as rigid and gas-phase fugacities were calculated using a Peng−Robinson equation of state (EOS)[58] with parameters taken from the NIST Chemistry WebBook[59] with the standard chemical potential calculated within the model for each temperature studied by performing NPT simulation at 1.0 bar. We have verified by direct NPT simulation at a few sample pressures that the errors introduced by the use of this EOS are not significant (the maximum deviation is less than 1%).

To complement the MC simulations, we also undertook calculations of the binding energies of a single CH_4 molecule as a function of its center of mass position within the ZIFs. Specifically, the binding energies of CH_4 were calculated for a single molecule in a single ZIF unit cell using the program Large-scale Atomic/Molecular Massively Parallel Simulator

dx.doi.org/10.1021/jp3096192 | J. Phys. Chem. C 2013, 117, 10326−10335

(LAMMPS).[60] Appropriate energies for the ZIF and molecule alone were subtracted to obtain binding energies. The binding energies were computed for a rectangular grid with steps $L/256$, where L is the length of a side of the cubic unit cell. The symmetries of the ZIF crystal structure were used to reduce the number of actual computations. For each binding position, the molecule was placed at the grid point and the energy computed without any relaxation of the atomic positions.

RESULTS

Adsorption of CH_4 at Low Pressure: Experiment and Molecular Modeling. The experimental CH_4 adsorption isotherms for the five ZIFs studied are shown in Figures 2 and 3

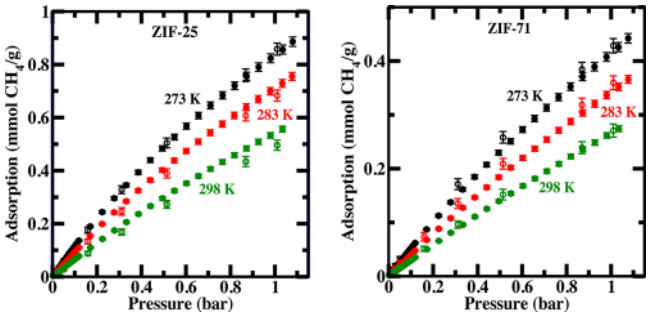

Figure 2. Comparison of experimental (closed circles) and calculated (open circles) CH_4 isotherms in ZIF-25 and -71 at 273, 283, and 298 K.

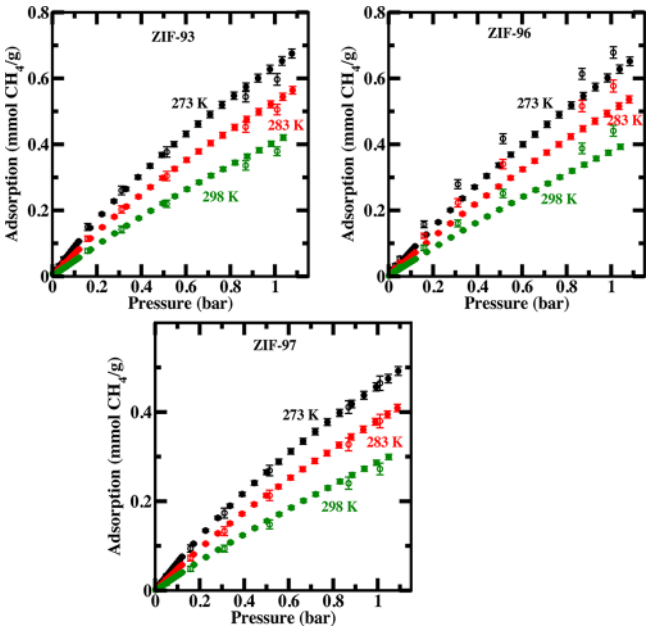

Figure 3. Comparison of experimental (closed circles) and calculated (open circles) CH_4 isotherms in ZIF-93, -96, and -97 at 273, 283, and 298 K.

for pressures up to 1 bar and three different temperatures (277, 283, and 298 K). Also shown are the corresponding isotherms from the GCMC simulation, which agree with experimentally measured values to within 13%, validating our chosen OPLS parameters for these systems. In our earlier work on CO_2 adsorption in this set of ZIFs,[27] we used the Universal Force Field (UFF) to describe the LJ parameters of the ZIF, which gave results showing comparable level of agreement with experimental measurements, with the exception of ZIF-96, for which the CO_2 adsorption was significantly underestimated. For CH_4, the predicted adsorption isotherms using the UFF force field exhibited deviations from the experimental measurements, with the computed adsorptions being over predicted by as much as 145%. Similar overestimation of CH_4 adsorption using an unmodified UFF force field has been observed in both ZIF-8 and -69.[31]

For a particular pressure and temperature, the adsorption of CH_4 varies by about a factor of 2 within this series. For example, at 1.00 bar and 298 K, we obtain CH_4 adsorptions of 0.556, 0.274, 0.421, 0.393, and 0.299 $mmol^{-1}$ for ZIF-25, -71, -93, -96, and -97, respectively. Because the ZIFs in this series have the same framework structure and adsorption in porous materials at low pressure depends primarily to adsorbent/guest interactions strength,[61] the differences in CH_4 sorption observed at low pressure is due to the variance of the functional groups in the ZIFs. Because the CH_4 model adopted in this work is uncharged, differences in the CH_4 in the ZIFs depend on differences in the van der Waals (vdW) interaction strength of the individual linker functionalities. Similar results were obtained for CH_4 sorption in an isoreticular ZIF series with sodalite (SOD) topology.[43]

In our previous work on CO_2 adsorption in this ZIF series,[27] the specific effect of the functional group was best seen by examining the adsorption relative to the BET surface area. (See Table 1 for the BET surface area values for this series.) For

Table 1. Structural and Physical Properties of the RHO Topology ZIFs Considered in This Work[a]

ZIF	BET surface area ($m^2\ g^{-1}$)	density ($g\ cm^{-3}$)	free volume ($cm^3\ g^{-1}$) (%)
25	1110	0.857	0.511 (43.8)
71	652	1.184	0.384 (45.5)
93	864	0.991	0.391 (38.8)
96	960	0.977	0.449 (43.9)
97	564	0.997	0.351 (35.0)

[a]The details associated with the calculation of the BET surface area can be found in ref 27. Densities are based on the crystal structure. The free volumes were calculated using the PLATON program[93] with a probe radius based on the methane diameter (3.73 Å).

CO_2 adsorption, RHO ZIFs with asymmetrically functionalized imidazolate linkers (-93, -96, and -97) had an adsorption per unit surface area that was approximately twice that of symmetrically functionalized ZIFs (-25 and -71) as shown in Figure 4. Also in Figure 4 we show the CH_4 adsorption per unit area from the current experimental data. Not only are these values smaller by a factor of 2−5 than that for CO_2 adsorption, they are by comparison with CO_2 roughly independent of functional group; therefore, CH_4 adsorption in this series is approximately proportional to BET surface area, in contrast to CO_2 adsorption. This is consistent with the hypothesis in ref 27 that the enhanced adsorption in asymmetric ZIFs was largely due to electrostatic considerations. This has important implications for the CO_2/CH_4 selectivity in this series as discussed below.

Adsorption of CH_4 at High Pressure: Molecular Modeling. To examine the adsorption uptake capacity of CH_4 in ZIFs, adsorption isotherms were calculated up to 80.0 bar by GCMC simulations. These high-pressure adsorption

dx.doi.org/10.1021/jp3096192 | J. Phys. Chem. C 2013, 117, 10326−10335

Table 2. LJ Potential Parameters for CH_4 and ZIFs

species	atom	ε/k_b (K)	σ (Å)
methane	CH_4	148.0	3.73
imidazolate ring	C	25.16	2.25
	N	85.55	3.25
	Zn	62.40	2.46
	H	15.10	2.50
functional groups	$C(CH_3)$	75.48	3.65
	$H(CH_3)$	15.10	2.50
	Cl	133.9	3.47
	C(CO)	25.16	2.55
	O(CO)	105.7	2.96
	H(HCO)	7.548	2.42
	$N(NH_2)$	85.55	3.15
	$H(NH_2)$	0.000	0.00
	C(CN)	105.7	3.30
	N(CN)	85.55	2.90
	C(COH)	33.21	3.50
	O(OH)	85.55	3.12
	H(HCOH)	0.000	0.00
	H(OH)	0.000	0.00

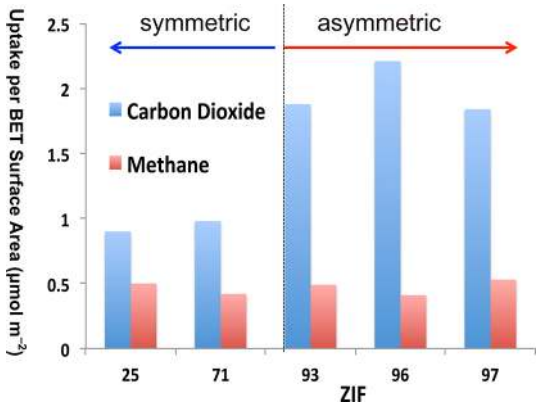

Figure 4. Experimental CH_4 and CO_2 adsorption per unit BET surface area for the five RHO ZIFs under study here. The ZIFs on the left side of the graph are symmetrically functionalized (-25 and -71), while those on the right (-93, -96, and -97) are asymmetrically functionalized at the imidazole 4 and 5 positions. The CO_2 adsorption data were taken from ref 27.

isotherms are shown in Figure 5 at three temperatures: 273, 283, and 298 K.

At all three temperatures and at all pressures studied, the CH_4 adsorption in this ZIF series shows a nearly factor-of-two variation with respect to functional group. In order of increasing adsorption, we have ZIF-71 < -97 < -93 < -96 < -25, independent of pressure. At a temperature of 298 K and the highest pressure studied (80.0 bar), the CH_4 adsorptions are 4.23, 4.45 5.23, 5.74, and 7.74 mmol g^{-1} for ZIF-71, -97, -93, -96, and -25, respectively, with corresponding volumetric adsorptions of 147, 126, 116, 99, and 112 v/v, respectively.

The amounts of CH_4 adsorbed in the ZIFs at high pressure correlate fairly well with the ZIFs' free volume displayed in Table 1, with the exception of ZIF-97, which has a slightly higher adsorption of CH_4 than ZIF-71 despite a slightly lower surface area (see Table 1). These results suggest that the dominant influence on adsorption of CH_4 in the ZIFs is BET

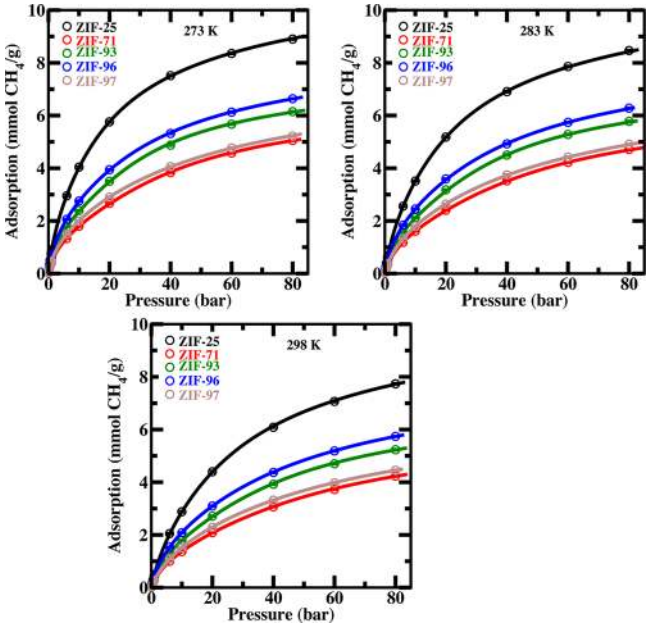

Figure 5. Simulated adsorption isotherms (open circle) of CH_4 in each ZIF at 273, 283, and 298 K. The solid lines represent fits using the virial-type expansion.

surface area or free volume, consistent with results obtained by the Snurr group[62] and Wang et al.,[63] but that there are smaller linker specific considerations that can be important when comparing two isoreticular ZIFs of similar surface area.[43,64] The uptakes observed at 40.0 bar reported in Figure 5 in the best performing materials, ZIF-25 (117 v/v) and ZIF-96 (96 v/v), are comparable to or better than those reported in other MOFs at 35.0 bar (128, 135, and 100 v/v for IRMOF-1, IRMOF-6, and IRMOF-14, respectively)[62] and ZIFs at 50.0 bar (120 v/v for ZIF-2 and ZIF-8, and 50, 55, and 75 v/v for ZIF-4, ZIF-5, and ZIF-9, respectively),[31,42] but they are lower than the methane capacity of 180 v/v at 35.0 bar set by the U.S. Department of Energy (DOE) for vehicular application.[65] Note that the saturation storage capacity of methane in all ZIFs studied is not reached at 80.0 bar.

Methane Isosteric Heats of Adsorption: Experiment and Molecular Modeling. To study CH_4–sorbent energetic interactions, we have calculated from GCMC simulations the isosteric heat of adsorption Q_{st} directly from the fluctuation of the total energy of the simulated system using eq 2:[66]

$$Q_{st} = RT - \frac{\langle \Phi N \rangle - \langle \Phi \rangle \langle N \rangle}{\langle N^2 \rangle - \langle N \rangle^2} \quad (2)$$

where Φ, N, T, and R are the potential energy of the adsorbed phase, the number of molecules adsorbed, temperature, and gas constant, respectively, and the angle brackets $\langle ... \rangle$ denote averaging. Q_{st} can also be estimated by a virial-type expansion that requires adsorption data at least at two, but preferably more, temperatures.[67−69]

$$\ln P = \ln N + \frac{1}{T}\sum_{i=0}^{m} a_i N^i + \sum_{i=0}^{n} b_i N^i \quad (3)$$

where P is the pressure, N is the adsorbed amount in mmol g^{-1}, T is the temperature, a_i and b_i are virial coefficients, and m and n are the number of required coefficients to adequately fit the isotherms. Equation 2 is convenient in simulation studies

dx.doi.org/10.1021/jp3096192 | J. Phys. Chem. C 2013, 117, 10326−10335

because it can be computed easily during GCMC simulation at a single temperature to allow rapid screening of ZIF materials.[66,70−73]

The experimental isosteric heats of adsorption estimated from the virial-type expansion at low pressure are plotted in Figure 6. Also plotted in Figure 6 are corresponding heats of

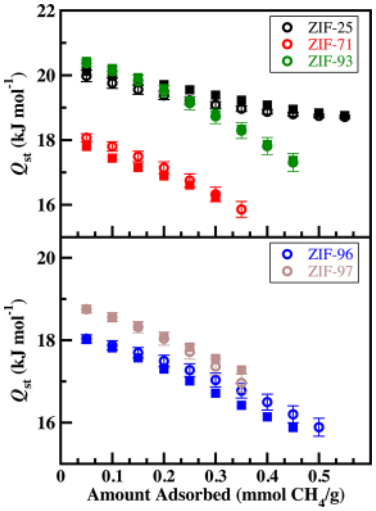

Figure 6. Estimated isosteric heat of adsorption as a function of CH_4 uptake from the virial-type expansion of the low-pressure experimental (filled squares) and simulation (open circles) adsorption data in ZIF-25 (black), -71 (red), -93 (green), -96 (blue), and -97 (brown) at 298 K.

adsorption values calculated using the virial-type expansion of the GCMC simulated isotherms at low pressure, which show agreement to within 3% of experimental measurements, validating once again our chosen OPLS parameters for these systems.

The isosteric heats of adsorption at 298 K, derived from simulations using eq 2, are plotted as a function of CH_4 loading with open symbols in Figure 7. For comparison, the heats of adsorption at 298 K estimated using the virial-type expansion are also shown, with solid lines, to illustrate the consistency of the two calculations. We have also calculated Q_{st} values at 273 and 298 K, but within the error bars of the calculation the isosteric heat of adsorption is found to be independent of the temperature over this range. The combined simulated isotherm data of the ZIFs at 273, 283, and 298 K was used for the virial expansion fitting to eq 3 with $m = 4$, $n = 3$. The fitted curves are represented by solid lines in Figure 5.

The sequence of Q_{st} values in the ZIFs at low CH_4 loading, averaged in the range 0−0.5 bar, is 19.9(2), 18.8(3), 18.2(2), 17.3(1), and 17.2(4) kJ mol^{-1} for ZIF-93, -25, -97, -71, and -96, respectively, where the numbers in parentheses are the estimated 95% confidence level errors in the last digits shown. The Q_{st} values obtained at low loading for methane in the ZIFs considered in this work are comparable to those reported for other MOF structures (18.7, 18.2, and 16.1 kJ mol^{-1} for Cu-BTC, HKUST-1, and CPL-2, respectively)[74,75] and ZIFs (15.52−20.5 kJ mol^{-1} for ZIF-68, -69, -70, -80, -81, -82).[31,76] For the RHO ZIFs considered in this work, the values of Q_{st} first decrease at low coverage, but then increase at higher CH_4 uptake. In previous studies,[77−79] the increase of Q_{st} at higher loading was attributed to guest−guest interactions (in this case, CH_4−CH_4). In addition, Sircar and Cao[79] reported

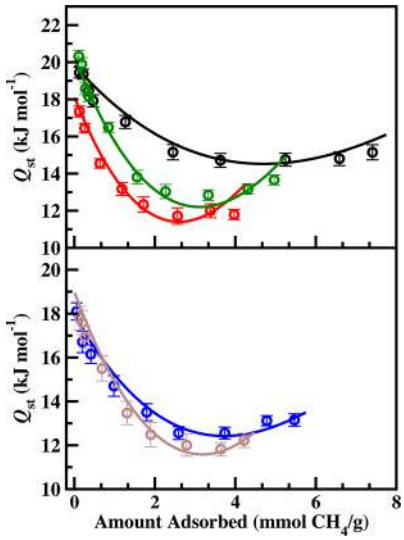

Figure 7. Calculated isosteric heat of adsorption as a function of CH_4 uptake in ZIF-25 (black), -71 (red), -93 (green), -96 (blue), and -97 (brown) at 298 K. The solid lines represent the estimated isosteric heat of adsorption from the virial-type expansion of the adsorption data.

that the decrease of the Q_{st} in ZIFs at low loading is due to energetic heterogeneity in the ZIF adsorption sites; that is, the guest gas molecules are first adsorbed in the strongest binding sites at low loading, as will be discussed further for our system in the following section. The decrease in Q_{st} at low coverage in the ZIFs has also been observed in other work for CO_2 and H_2.[40,45,48]

At high loading (40.0−80.0 bar), the average values for the calculated heats of adsorption are 15.0(2), 13.4(3), 13.2(1), 12.0(2) and 11.8(2) kJ mol^{-1} for ZIF-25, -93, -96, -97 and -71, respectively, in order of decreasing Q_{st}. These values are comparable to those found in other MOFs (about 12.0 kJ mol^{-1} in IRMOF-1)[80] and ZIFs (12.0−15.2 kJ mol^{-1})[64] at high loading. Furthermore, the steady increase of Q_{st} in the high uptake regime is consistent with the observation that the saturation capacity is not reached at 80.0 bar.

CH_4 Adsorption Sites. To examine the main adsorption sites for methane in the RHO ZIFs considered in this work, we have computed the binding energy as a function of the center of mass (COM) position of a CH_4 molecule, as described in the Methodology section. In Figure 8a, the results are presented by contour plots in a slice through the structure corresponding to a (110) plane through the middle of the α-cavity indicated by the yellow sphere in Figure 1. Similar to the analysis for CO_2 adsorption in ref 81, we identify three sets of binding sites: one between the ZIF linkers in the six-membered ring window of the α-cavity, another in the connecting double 8-rings, and a final set on the inner surface of the α-cavities near to the four-membered ring. The maximum binding energies in each of these sites are listed in Table 3. We find that the binding site confined to the six-membered ring window is the strongest in each of the ZIFs considered in this work, indicating that this site should dominate adsorption in the dilute limit.

We have further computed the COM of CH_4 probability distribution directly from the GCMC simulations. The two-dimensional distributions at 298 K are plotted in Figure 9 for low (0.514 bar) and moderate (40.0 bar) pressures. These data are consistent with the three adsorption sites described above,

dx.doi.org/10.1021/jp3096192 | J. Phys. Chem. C 2013, 117, 10326−10335

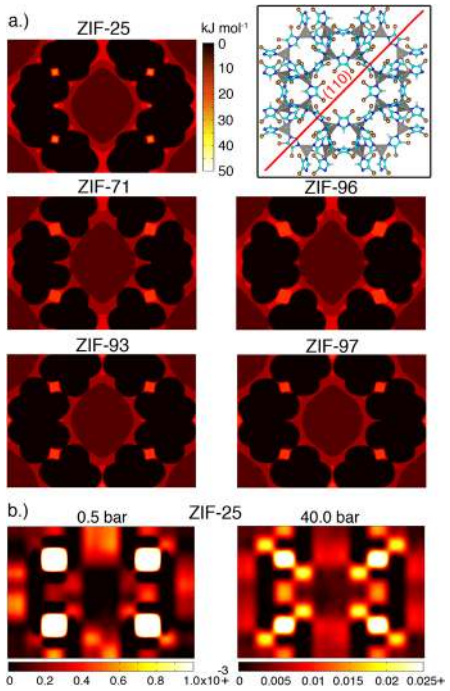

Figure 8. (a) Methane binding energy as a function of position in the (110) plane in kJ mol^{-1}. (b) Methane density maps in the (110) plane of ZIF-25 for 0.514 and 40.0 bar in number of molecules per Å^3. Inset: ZIF-71 viewed along the [001] direction. The projection of the (110) plane in which the binding-energy and density maps are plotted is shown by the red line. This plane cuts through the center of the main pore in the RHO structure.

Table 3. Maximum CH_4 Binding Energies by Binding Site[a]

	binding energy (kJ mol^{-1})		
ZIF	site A	site B	site C
25	24.65	16.15	18.63
71	19.94	14.36	11.48
93	21.39	18.74	11.72
96	20.00	14.92	6.30
97	21.27	18.31	10.49

[a]Site A refers to the six-membered ring window of the α-cavity, site B refers to the connecting double 8-rings, and site C refers to the inner surface of the α-pore near to the four-membered ring, as discussed in the text.

as made clear in Figure 8b. Here, a slice along the (110) plane of the CH_4 density in ZIF-25 at low and high pressure shows that the largest methane density is found near areas shown to have strong binding in Figure 8a. At low pressure, CH_4 molecules are primarily adsorbed between the ZIFs linkers in the six-membered ring window of the α cavities, consistent with the binding energy results. A comparatively small methane population is also present in the connecting double 8-rings. With increasing pressure, methane continues populating these two sites and distributes throughout the connecting double 8-rings. In addition, the inner surfaces of the α cavities begin to host larger methane concentrations, both in the ⟨110⟩ direction as well as at the entrance to the six-membered ring window. At high pressure, these sites continue to carry an increasing proportion of the methane load. Specifically, when increasing the pressure from 0.514 to 40.0 bar the densities in the six-ring site increase by roughly a factor of 5, the density in the 8-rings

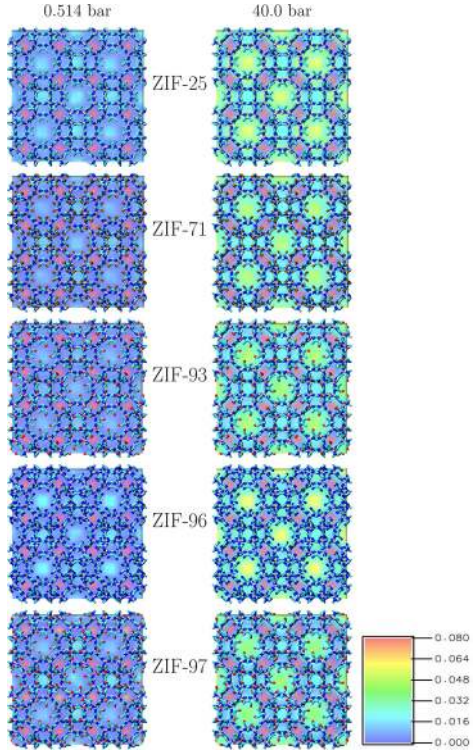

Figure 9. Probability density averaged over unit cells in the *XY* plane as a function of the center of mass (COM) of CH_4 in each ZIF at 298 K for different pressures: left, 0.514 bar; right, 40.0 bar. The density is in number of molecules per Å^3. The scale for 0.514 bar is a factor of 8 smaller than that for 40.0 bar. Atom colors: zinc, silver; carbon, cyan; nitrogen, blue; oxygen, red; chlorine, ochre. Hydrogen atoms are omitted for clarity.

by a factor of 18, and the density on the inner surface of the pore by a factor of 52.

With increasing pressure, there is a shift in the fraction of the adsorbed methane at the different sites: at low pressure the majority of the adsorbed methane resides in the small-volume/high-binding-energy sites, while at high pressures more methane is found in the more weakly bound sites that are open to empty space within the pores.

Equilibrium CO_2/CH_4 Selectivity. We conclude this section by considering the equilibrium selectivity of CO_2 versus CH_4 (defined in the Supporting Information) in the RHO ZIFs considered in this work. To calculate the equilibrium selectivity for an equimolar mixture of CO_2/CH_4 from the pure gas experimental adsorption data we employ IAST, which has been shown to give good prediction of the adsorption selectivity in MOFs[82−84] and ZIFs.[34,35,38] In these calculations, we use the CH_4 experimental data from the current study as well as the pure CO_2 data from our previous work on CO_2 in this series.[27] The IAST selectivity and the fitting parameters for CO_2 and CH_4 adsorptions in the ZIFs can be found in the Supporting Information.

From our IAST analysis, the CO_2/CH_4 equilibrium selectivities at 1 bar and 298 K are calculated to be 2.53, 2.67, 8.19, 10.20, and 6.14 for ZIF-25, -71, -93, -96, and -97, respectively. The ZIFs with the highest low-pressure selectivities of this group (-93, -96, and -97) are those with asymmetrically functionalized imidazolate linkers and are among the higher values reported for other MOFs and ZIFs.[23,34,35,42,43,85] This is as expected from our observation

dx.doi.org/10.1021/jp3096192 | J. Phys. Chem. C 2013, 117, 10326−10335

in the current work that the adsorption of CH_4 in this ZIF RHO series is roughly proportional to BET surface area, independent of functional group, combined with our earlier observation[27] that noncanceling electrostatic interactions in the asymmetrically functionalized RHO ZIFs (-93, -96, and -97) lead to an enhanced adsorption per unit BET surface area over the symmetrically functionalized ZIFs (-25 and -71)

In a similar study on an isoreticular series, Amrouche et al.[43] examined a similar series of ZIFs with a SOD topology. In this series, the imidazolate was singly functionalized at the 2 position (as opposed to the 4 and 5 positions functionalized in the current RHO series) and a strong correlation was observed between the selectivity and the dipole moment of the functional group - consistent with our observations in the RHO series that optimizing electrostatic interactions is crucial for designing ZIFs that have high CO_2/CH_4 selectivity. Given that the SOD series ZIFs were singly functionalized, the symmetry of functionalization was not an issue. The current work adds the symmetry of functionalization to the list of known parameters that affect CO_2/CH_4 equilibrium selectivity, such as the dipole-moment or polarizability of the adsorbed gases or the framework decoration[38,43,82,86−91] or framework flexibility.[92]

SUMMARY

We have examined, both experimentally and computationally, the methane adsorption of five zeolitic imidazolate framework (ZIF) materials: ZIF-25, -71, -93, -96, and -97. These ZIFs have identical RHO topology but different functionalization of the imidazole linker. Previously,[27] we have examined this same ZIF series for CO_2 adsorption. At low pressure (up to 1 bar), we find that that CH_4 adsorption in each ZIF is smaller (by factors ranging from 2.4 to 7.5) than the corresponding CO_2 adsorption at each pressure. In particular, we note that the CH_4 adsorption in these ZIFs is roughly proportional to the BET surface area, independent of functionalization. This is in contrast to our previous results for CO_2 adsorption[27] where there was a factor of 2 enhancement in the uptake per surface area for asymmetrically functionalized ZIFs (ZIF-93, -96, -97) over symmetrically functionalized ZIFs (ZIF-25, -71). In that work, we hypothesized that the enhancement was due to electrostatic effects. The absence of such enhancement in the CH_4 adsorption data, for which electrostatics play a minimal role, is consistent with that hypothesis. Because of the enhancement of CO_2 adsorption in the asymmetric ZIFs, these ZIFs show considerably better selectivity of CO_2 over CH_4 than is observed in the symmetric ZIFs. The observation that electrostatic interactions play a dominant role in determining CO_2/CH_4 selectivity in ZIFs is consistent with the results from earlier works.[23,24,31,35,39,42,43]

To analyze gas uptake at the molecular level, we have modeled the adsorption using grand canonical Monte Carlo simulation at both low and high pressures. At low pressures, the simulated adsorptions are in excellent agreement with the experiments, validating our model for the interatomic interactions. Our high-pressure simulations show no change in the relative ordering of the ZIFs in the series with respect to adsorption and also show that the saturation pressure for CH_4 for all ZIFs studied is not yet reached at the maximum pressure considered, 80 bar. Isosteric heats of adsorption, Q_{st}, were also calculated from both the experimental and simulated adsorption data. For all ZIFs, Q_{st} shows an initial decrease at low loadings and an increased at high loadings, as CH_4-CH_4 interactions become more important. At higher pressures, the simulations show that Q_{st} goes through a minimum and begins to increase at higher loadings. These results were further investigated through an analysis of the binding energies and density profiles within the ZIF structures. We found from the analysis of the binding energy that the higher binding energy sites for CH_4 in the ZIFs are located between the ZIF linkers in the six-membered ring and the lower binding energy sites are in the connecting double 8-rings and also in the inner surface of the pore close to the four-membered ring. The density profiles analysis shows that at low pressures methane molecules adsorb preferentially in the higher binding energy sites, while at high pressures a higher fraction of the methane molecules are found at lower binding energy sites that feature larger available volumes.

ASSOCIATED CONTENT

Supporting Information

Table of the dual-site Langmuir−Freundlich model fitting parameters for the CO_2 and CH_4 adsorptions in the ZIFs; figure of IAST adsorption selectivity of CO_2 in ZIFs at 298 K for gas mixture of CO_2/CH_4 50/50. This material is available free of charge via the Internet at http://pubs.acs.org/.

AUTHOR INFORMATION

Corresponding Author

*E-mail: yhoundonoug@ewu.edu. Phone: 509-359-4332. Fax: 509-359-6973.

Notes

The authors declare no competing financial interest.

ACKNOWLEDGMENTS

This material is based upon work supported as part of the Molecularly Engineered Energy Materials, an Energy Frontier Research Center funded by the U.S. Department of Energy, Office of Science, Office of Basic Energy Sciences under Award Number DE-SC0001342. This work made use of the High Performance Computing resources provided by the Eastern Washington University.

REFERENCES

(1) Celzard, A.; Fierro, V. Preparing a Suitable Material Designed for Methane Storage: A Comprehensive Report. *Energy Fuels* **2005**, *19*, 573−583.

(2) Aaron, D.; Tsouris, C. Separation of CO_2 from Flue Gas: A Review. *Sep. Sci. Technol.* **2005**, *40*, 321−348.

(3) Mendoza-Cortes, J. L.; Han, S. S.; Furukawa, H.; Yaghi, O. M.; Goddard, W. A., III. Adsorption Mechanism and Uptake of Methane in Covalent Organic Frameworks: Theory and Experiment. *J. Phys. Chem. A* **2010**, *114*, 10824−10833.

(4) Ribeiro, A. M.; Santos, J. C.; Rodrigues, A. E.; Rifflart, S. Pressure Swing Adsorption Process in Coal to Fischer−Tropsch Fuels with CO2 Capture. *Energy Fuels* **2012**, *26*, 1246−1253.

(5) Rosi, N.; Eckert, J.; Eddaoudi, M.; Vodak, D.; Kim, J.; O'Keeffe, M.; Yaghi, O. Hydrogen Storage in Microporous Metal-Organic Frameworks. *Science* **2003**, *300*, 1127−1129.

(6) Li, J.-R.; Kuppler, R. J.; Zhou, H.-C. Selective Gas Adsorption and Separation in Metal-Organic Frameworks. *Chem. Soc. Rev.* **2009**, *38*, 1477−1504.

(7) Rowsell, J.; Yaghi, O. Metal-Organic Frameworks: a New Class of Porous Materials. *Microporous Mesoporous Mater.* **2004**, *73*, 3−14.

(8) Rowsell, J.; Yaghi, O. Effects of Functionalization, Catenation, and Variation of the Metal Oxide and Organic Linking Units on the Low-Pressure Hydrogen Adsorption Properties of Metal-Organic Frameworks. *J. Am. Chem. Soc.* **2006**, *128*, 1304−1315.

(9) Kaye, S. S.; Dailly, A.; Yaghi, O. M.; Long, J. R. Impact of Preparation and Handling on the Hydrogen Storage Properties of Zn_4O(1,4-benzenedicarboxylate)$_3$ (MOF-5). *J. Am. Chem. Soc.* **2007**, *129*, 14176−14177.
(10) Furukawa, H.; Ko, N.; Go, Y. B.; Aratani, N.; Choi, S. B.; Choi, E.; Yazaydin, A. O.; Snurr, R. Q.; O'Keeffe, M.; Kim, J.; Yaghi, O. M. Ultrahigh Porosity in Metal-Organic Frameworks. *Science* **2010**, *329*, 424−428.
(11) Saha, D.; Deng, S. Structural Stability of Metal Organic Framework MOF-177. *J. Phys. Chem. Letters* **2010**, *1*, 73−78.
(12) Kang, I. J.; Khan, N. A.; Haque, E.; Jhung, S. H. Chemical and Thermal Stability of Isotypic Metal-Organic Frameworks: Effect of Metal Ions. *Chem.—Eur. J.* **2011**, *17*, 6437−6442.
(13) Park, K. S.; Ni, Z.; Coté, A. P.; Choi, J. Y.; Huang, R.; Uribe-Romo, F. J.; Chae, H. K.; O'Keeffe, M.; Yaghi, O. M. Exceptional Chemical and Thermal Stability of Zeolitic Imidazolate Frameworks. *Proc. Natl. Acad. Sci. U.S.A.* **2006**, *103*, 10186−10191.
(14) Banerjee, R.; Phan, A.; Wang, B.; Knobler, C.; Furukawa, H.; O'Keeffe, M.; Yaghi, O. M. High-Throughput Synthesis of Zeolitic Imidazolate Frameworks and Application to CO2 Capture. *Science* **2008**, *319*, 939−943.
(15) Banerjee, R.; Furukawa, H.; Britt, D.; Knobler, C.; O'Keeffe, M.; Yaghi, O. M. Control of Pore Size and Functionality in Isoreticular Zeolitic Imidazolate Frameworks and their Carbon Dioxide Selective Capture Properties. *J. Am. Chem. Soc.* **2009**, *131*, 3875−3877.
(16) Phan, A.; Doonan, C. J.; Uribe-Romo, F. J.; O'Keefe, C. B. K. M.; Yaghi, O. M. Synthesis, Structure, and Carbon Dioxide Capture Properties of Zeolitic Imidazolate Frameworks. *Acc. Chem. Res.* **2010**, *43*, 58−67.
(17) Keskin, S.; Sholl, D. S. Screening Metal-Organic Framework Materials for Membrane-Based Methane/Carbon Dioxide Separations. *J. Chem. Phys. C. Lett* **2007**, *111*, 14055−14059.
(18) Bux, H.; Liang, F.; Li, Y.; Cravillon, J.; Wiebcke, M.; Caro, J. Zeolitic Imidazolate Framework Membrane with Molecular Sieving Properties by Microwave-Assisted Solvothermal Synthesis. *J. Am. Chem. Soc.* **2009**, *131*, 16000.
(19) Bae, T.-H.; Lee, J. S.; Qiu, W.; Koros, W. J.; Jones, C. W.; Nair, S. A High-Performance Gas-Separation Membrane Containing Submicrometer-Sized Metal-Organic Framework Crystals. *Angew. Chem., Int. Ed.* **2010**, *49*, 9863−9866.
(20) Huang, A.; Dou, W.; Caro, J. Steam-Stable Zeolitic Imidazolate Framework ZIF-90 Membrane with Hydrogen Selectivity through Covalent Functionalization. *J. Am. Chem. Soc.* **2010**, *132*, 15562−15564.
(21) Li, Y.-S.; Liang, F.-Y.; Bux, H.; Feldhoff, A.; Yang, W.-S.; Caro, J. Molecular Sieve Membrane: Supported Metal-Organic Framework with High Hydrogen Selectivity. *Angew. Chem., Int. Ed.* **2010**, *49*, 548−551.
(22) Li, Y.; Liang, F.; Bux, H.; Yang, W.; Caro, J. Zeolitic Imidazolate Framework ZIF-7 Based Molecular Sieve Membrane for Hydrogen Separation. *J. Membr. Sci.* **2010**, *354*, 48−54.
(23) Liu, Y.; Liu, D.; Yang, Q.; Zhong, C.; Mi, J. Comparative Study of Separation Performance of COFs and MOFs for $CH_4/CO_2/H_2$ Mixtures. *Ind. Eng. Chem. Res.* **2010**, *49*, 2902−2906.
(24) Liu, Z.; Grande, C. A.; Li, P.; Yu, J.; Rodrigues, A. E. Multi-bed Vacuum Pressure Swing Adsorption for carbon dioxide capture from flue gas. *Sep. Purif. Technol.* **2011**, *81*, 307−317.
(25) Venna, S. R.; Carreon, M. A. Highly Permeable Zeolite Imidazolate Framework-8 Membranes for CO_2/CH_4 Separation. *J. Am. Chem. Soc.* **2010**, *132*, 76.
(26) Thornton, A. W.; Dubbeldam, D.; Liu, M. S.; Ladewig, B. P.; Hill, A. J.; Hill, M. R. Feasibility of Zeolitic Imidazolate Framework Membranes for Clean Energy Applications. *Energy Environ. Sci.* **2012**, *5*, 7637−7646.
(27) Morris, W.; Leung, B.; Furukawa, H.; Yaghi, O. K.; He, N.; Hayashi, H.; Houndonougbo, Y.; Asta, M.; Laird, B. B.; Yaghi, O. M. A Combined Experimental-Computational Investigation of Carbon Dioxide Capture in a Series of Isoreticular Zeolitic Imidazolate Frameworks. *J. Am. Chem. Soc.* **2010**, *132*, 11006−11008.
(28) Zhou, W.; Wu, H.; Hartman, M. R.; Yildirim, T. Hydrogen and Methane Adsorption in Metal-Organic Frameworks: A High-Pressure Volumetric Study. *J. Chem. Phys. C* **2007**, *111*, 16131−16137.
(29) Wu, H.; Zhou, W.; Yildirim, T. Methane Sorption in Nanoporous Metal-Organic Frameworks and First-Order Phase Transition of Confined Methane. *J. Chem. Phys. C* **2009**, *113*, 3029−3035.
(30) Pantatosaki, E.; Pazzona, F. G.; Megariotis, G.; Papadopoulos, G. K. Atomistic Simulation Studies on the Dynamics and Thermodynamics of Nonpolar Molecules within the Zeolite Imidazolate Framework-8. *J. Phys. Chem. B* **2010**, *114*, 2493−2503.
(31) Pérez-Pellitero, J.; Amrouche, H.; Siperstein, F.; Pirngruber, G.; Nieto-Draghi, C.; Chaplais, G.; Simon-Masseron, A.; Bazer-Bachi, D.; Peralta, D.; Bats, N. Adsorption of CO_2, CH_4, and N_2 on Zeolitic Imidazolate Frameworks: Experiments and Simulations. *Chem.—Eur. J.* **2010**, *16*, 1560−1571.
(32) Babarao, R.; Dai, S.; Jiang, D.-e. Effect of Pore Topology and Accessibility on Gas Adsorption Capacity in Zeolitic-Imidazolate Frameworks: Bringing Molecular Simulation Close to Experiment. *J. Phys. Chem. C* **2011**, *115*, 8126−8135.
(33) Huang, H.; Zhang, W.; Liu, D.; Liu, B.; Chen, G.; Zhong, C. Effect of Temperature on Gas Adsorption and Separation in ZIF-8: A Combined Experimental and Molecular Simulation Study. *Chem. Eng. Sci.* **2011**, *66*, 6297−6305.
(34) Keskin, S. Atomistic Simulations for Adsorption, Diffusion, and Separation of Gas Mixtures in Zeolite Imidazolate Frameworks. *J. Phys. Chem. C* **2011**, *115*, 800−807.
(35) Keskin, S. High CO_2 Selectivity of A Microporous Metal-Imidazolate Framework: A Molecular Simulation Study. *Ind. Eng. Chem. Res.* **2011**, *50*, 8230−8236.
(36) Krishna, R.; van Baten, J. M. In Silico Screening of Metal-Organic Frameworks in separation applications. *Phys. Chem. Chem. Phys.* **2011**, *13*, 10593−10616.
(37) Wang, X.-S.; Ma, S.; Rauch, J. M., K.; Simmons; Yuan, D.; Wang, X.-S.; Yildirim, T.; Cole, W. C.; Lopez, J. J.; De Meijere, A.; Zhou, H.-C. Metal-Organic Frameworks Based on Double-Bond-Coupled Di-Isophthalate Linkers with High Hydrogen and Methane Uptakes. *Chem. Mater.* **2008**, *20*, 3145−3152.
(38) Liu, B.; Smit, B. Molecular Simulation Studies of Separation of CO_2/N_2, CO_2/CH_4, and CH_4/N_2 by ZIFs. *J. Phys. Chem. C* **2010**, *114*, 8515−8522.
(39) Li, B.; Wei, S.; Chen, L. Molecular Simulation of CO_2, N_2 and CH_4 Adsorption and Separation in ZIF-78 and ZIF-79. *Mol. Sim.* **2011**, *37*, 1131−1142.
(40) Rankin, R. B.; Liu, J.; Kulkarni, A. D.; Johnson, J. K. Adsorption and Diffusion of Light Gases in ZIF-68 and ZIF-70: A Simulation Study. *J. Chem. Phys. C* **2009**, *113*, 16906−16914.
(41) Atci, E.; Keskin, S. Understanding the Potential of Zeolite Imidazolate Framework Membranes in Gas Separations Using Atomically Detailed Calculations. *J. Chem. Phys. C.* **2012**, *116*, 15525−15537.
(42) Battisti, A.; Taioli, S.; Garberoglio, G. Zeolitic Imidazolate Frameworks for Separation of Binary Mixtures of CO_2, CH_4, N_2 and H_2: A Computer Simulation Investigation. *Microporous Mesoporous Mater.* **2011**, *143*, 46−53.
(43) Amrouche, H.; Aguado, S.; Perez-Pellitero, J.; Chizallet, C.; Siperstein, F.; Farrusseng, D.; Bats, N.; Nieto-Draghi, C. Experimental and Computational Study of Functionality Impact on Sodalite-Zeolitic Imidazolate Frameworks for CO_2 Separation. *J. Phys. Chem. C* **2011**, *115*, 16425−16432.
(44) Allen, M.; Tildesley, D. *Computer Simulation of Liquids*; Oxford Science Press: Oxford, 1987.
(45) Morris, W.; He, N.; Ray, K. G.; Klonowski, P.; Furukawa, H.; Daniels, I. N.; Houndonougbo, Y. A.; Asta, M.; Yaghi, O. M.; Laird, B. B. A Combined Experimental-Computational Study on the Effect of Topology on Carbon Dioxide Adsorption in Zeolitic Imidazolate Frameworks. *J. Chem. Phys. C* **2012**, *116*, 24084−24090.
(46) Liu, D.; Zheng, C.; Yang, Q.; Zhong, C. Understanding the Adsorption and Diffusion of Carbon Dioxide in Zeolitic Imidazolate

Frameworks: A Molecular Simulation Study. *J. Chem. Phys. C* **2009**, *113*, 5004−5009.
(47) Zhou, M.; Wang, Q.; Zhang, L.; Liu, Y.-C.; Kang, Y. Adsorption Sites of Hydrogen in Zeolitic Imidazolate Frameworks. *J. Phys. Chem. B* **2009**, *113*, 11049−11053.
(48) Han, S. S.; Choi, S.-H.; Goddard, W. A., III. Zeolitic Imidazolate Frameworks as H-2 Adsorbents: Ab Initio Based Grand Canonical Monte Carlo Simulation. *J. Phys. Chem. C* **2010**, *114*, 12039−12047.
(49) Han, S. S.; Kim, D.; Jung, D. H.; Cho, S.; Choi, S.-H.; Jung, Y. Accurate Ab Initio-Based Force Field for Predictive CO_2 Uptake Simulations in MOFs and ZIFs: Development and Applications for MTV-MOFs. *J. Phys. Chem. C* **2012**, *116*, 20254−20261.
(50) McDaniel, J. G.; Schmidt, J. R. Robust, Transferable, and Physically Motivated Force Fields for Gas Adsorption in Functionalized Zeolitic Imidazolate Frameworks. *J. Phys. Chem. C* **2012**, *116*, 14031−14039.
(51) McDaniel, J. G.; Yu, K.; Schmidt, J. R. Ab Initio, Physically Motivated Force Fields for CO_2 Adsorption in Zeolitic Imidazolate Frameworks. *J. Phys. Chem. C* **2012**, *116*, 1892−1903.
(52) Stubbs, J. M.; Potoff, J. J.; Siepmann, J. I. Transferable Potentials for Phase Equilibria. 6. United-Atom Description for Ethers, Glycols, Ketones, and Aldehydes. *J. Phys. Chem. B* **2004**, *108*, 17596.
(53) Kaminski, G. A.; Friesner, R. A.; Tirado-Rives, J.; Jorgensen, W. L. Evaluation and Reparametrization of the OPLS-AA Force Field for Proteins via Comparison with Accurate Quantum Chemical Calculations on Peptides. *J. Phys. Chem. B* **2001**, *105*, 6474−6487.
(54) Jorgensen, W. L.; Maxwell, D. S.; Tirado-Rives, J. Development and Testing of the OPLS All-Atom Force Field on Conformational Energetics and Properties of Organic Liquids. *J. Am. Chem. Soc.* **1996**, *117*, 11225−11236.
(55) Rappe, A. K.; Casewit, C. J.; Colwell, K. S.; Goddard, I.; Skiff, W. A.; UFF, W. M. a Full Periodic Table Force Field for Molecular Mechanics and Molecular Dynamics Simulations. *J. Am. Chem. Soc.* **1992**, *114*, 10024−10035.
(56) Martin, M. G.; Chen, B.; Wick, C. D.; Potoff, J. J.; Stubbs, J. M.; Siepmann, J. I. *MCCCS Towhee*; http://towhee.sourceforge.net.
(57) McDonald, I. NpT-Ensemble Monte Carlo Calculations for Binary Liquid Mixtures. *Mol. Phys.* **1972**, *23*, 41−58.
(58) Peng, D.; Robinson, D. A New Two-Constant Equation of State. *Ind. Eng. Chem. Fundam.* **1976**, *15*, 59.
(59) http://webbook.nist.gov/chemistry.
(60) Plimpton, S.; Fast, S. Parallel Algorithms for Short-Range Molecular Dynamics. *J. Comput. Phys.* **1995**, *117*, 1−19.
(61) Frost, H.; Duren, T.; Snurr, R. Effects of Surface Area, Free Volume, and Heat of Adsorption on Hydrogen Uptake in Metal-Organic Frameworks. *J. Phys. Chem. B* **2006**, *110*, 9565−9570.
(62) Duren, T.; Sarkisov, L.; Yaghi, O. M.; Snurr, R. Q. Design of New Materials for Methane Storage. *Langmuir* **2004**, *20*, 2683−2689.
(63) Wang, C.; Bradley, P.; Baker, D. Protein-Protein Docking with Backbone Flexibility. *J. Mol. Biol.* **2007**, *373*, 503.
(64) Guo, H.-C.; Shi, F.; Ma, Z.-F.; Liu, X.-Q. Molecular Simulation for Adsorption and Separation of CH_4/H_2 in Zeolitic Imidazolate Frameworks. *J. Phys. Chem. C* **2010**, *114*, 12158−12165.
(65) Burchell, T.; Rogers, M. Low Pressure Storage of Natural Gas for Vehicular Applications. *SAE Tech. Pap. Ser.* **2000**, *01*, 2000−2205.
(66) Snurr, R. Q.; Bell, A. T.; Theodorou, D. N. Prediction of Adsorption of Aromatic Hydrocarbons in Silicalite from Grand Canonical Monte Carlo Simulations with Biased Insertions. *J. Phys. Chem.* **1993**, *97*, 13742−13752.
(67) Czepirski, L.; Jagiello, J. Virial-Type Thermal Equation of Gas-Solid Adsorption. *Chem. Eng. Sci.* **2007**, *44*, 797−801.
(68) Jagiello, J.; Bandosz, T. J.; Putyera, K.; Schwarz, J. A. Adsorption near Ambient Temperatures of Methane, Carbon Tetrafluoride, and Sulfur Hexafluoride on Commercial Activated Carbons. *J. Chem. Eng. Data* **1995**, *40*, 1288−1292.
(69) Furukawa, H.; Miller, M. A.; Yaghi, O. M. Independent Verification of the Saturation Hydrogen Uptake in MOF-177 and Establishment of a Benchmark for Hydrogen Adsorption in Metal-Organic Frameworks. *J Mater. Chem.* **2007**, *17*, 3197−3204.
(70) Getman, R. B.; Bae, Y.-S.; Wilmer, C. E.; Snurr, R. Q. Review and Analysis of Molecular Simulations of Methane, Hydrogen, and Acetylene Storage in Metal-Organic Frameworks. *Chem. Rev.* **2012**, *112*, 703−723.
(71) Coasne, B.; Galarneau, A.; Di Renzo, F.; Pellenq, R. J. M. Molecular Simulation of Nitrogen Adsorption in Nanoporous Silica. *Langmuir* **2010**, *26*, 10872−10881.
(72) Vlugt, T. J. H.; Garcia-Perez, E.; Dubbeldam, D.; Ban, S.; Calero, S. Computing the Heat of Adsorption Using Molecular Simulations: The Effect of Strong Coulombic Interactions. *J. Chem. Theory Comput.* **2008**, *4*, 1107−1118.
(73) Heuchel, M.; Snurr, R.; Buss, E. Adsorption of CH_4−CF_4 Mixtures in Silicalite: Simulation, Experiment, and Theory. *Langmuir* **1997**, *13*, 6795−6804.
(74) Wang, S. Comparative Molecular Simulation Study of Methane Adsorption in Metal-Organic Frameworks. *Energy Fuels* **2007**, *21*, 953−956.
(75) Senkovska, I.; Kaskel, S. High Pressure Methane Adsorption in the Metal-Organic Frameworks Cu-3$(btc)_2$, $Zn_2(bdc)_2$dabco, and $Cr_3F(H_2O)_2O(bdc)_3$. *Microporous Mesoporous Mater.* **2008**, *112*, 108−115.
(76) Ye, Q.; Yan, S.; Liu, D.; Yang, Q.; Zhong, C. Methane Adsorption in Several Series of Newly Synthesised Metal-Organic Frameworks: a Molecular Simulation Study. *Mol. Sim.* **2010**, *36*, 682−692.
(77) Bakaev, V. A.; Bakaeva, T. I.; Pantano, C. G. On Inverse Adsorption Chromatography. 2. Determination of Isotherms and Heats of Adsorption as Well as Energy Distributions of Adsorption Sites. *J. Chem. Phys. C* **2007**, *111*, 7473−7486.
(78) Goj, A.; Sholl, D. S.; Akten, E. D.; Kohen, D. Atomistic Simulations of CO_2 and N_2 Adsorption in Silica Zeolites: The Impact of Pore Size and Shape. *J. Phys. Chem. B* **2002**, *106*, 8367−8375.
(79) Sircar, S.; Cao, D. V. Heat of Adsorption. *Chem. Eng. Technol.* **2002**, *10*, 945−948.
(80) Babarao, R.; Hu, Z.; Jiang, J.; Chempath, S.; Sandler, S. I. Storage and Separation of CO_2 and CH_4 in Silicalite, C-168 Schwarzite, and IRMOF-1: A Comparative Study from Monte Carlo Simulation. *Langmuir* **2007**, *23*, 659−666.
(81) Ray, D., K. G.; Olmsted, N., H.; Houndonougbo, Y.; Laird, B. B.; Asta, M. van der Waals Density Functional Study of CO_2 Binding in Zeolitic Imidazolate Frameworks. *Phys. Rev. B* **2012**, *85*, 085410−085418.
(82) Zhang, Z.; Li, Z.; Li, J. Computational Study of Adsorption and Separation of CO_2, CH_4, and N_2 by an rht-Type Metal-Organic Framework. *Langmuir* **2012**, *28*, 12122−12133.
(83) Moellmer, J.; Lange, M.; Moeller, A.; Patzschke, C.; Stein, K.; Laessig, D.; Lincke, J.; Glaeser, R.; Krautscheid, H.; Staudt, R. Pure and Mixed Gas Adsorption of CH_4 and N_2 on the Metal-Organic Framework Basolite (R) A100 and a Novel Copper-Based 1,2,4-triazolyl isophthalate MOF. *J. Mater. Chem.* **2012**, *22*, 10274−10286.
(84) Zhang, Z.; Liu, J.; Li, Z.; Li, J. Experimental and Theoretical Investigations on the MMOF Selectivity for CO_2 vs. N_2 in Flue Gas Mixtures. *Dalton Trans.* **2012**, *41*, 4232−4238.
(85) Atci, E.; Erucar, I.; Keskin, S. Adsorption and Transport of CH_4, CO_2, H_2 Mixtures in a Bio-MOF Material from Molecular Simulations. *J. Phys. Chem. C* **2011**, *115*, 6833−6840.
(86) Xiang, Z.; Peng, X.; Cheng, X.; Li, X.; Cao, D. CNT@Cu-3$(BTC)_2$ and Metal-Organic Frameworks for Separation of CO_2/CH_4 Mixture. *J. Chem. Phys. C* **2011**, *115*, 19864−19871.
(87) Reich, T. E.; Behera, S.; Jackson, K. T.; Jena, P.; El-Kaderi, H. M. Highly Selective CO_2/CH_4 Gas Uptake by a Halogen-Decorated Borazine-Linked Polymer. *J Mater. Chem.* **2012**, *22*, 13524−13528.
(88) Xu, Q.; Liu, D.; Yang, Q.; Zhong, C.; Mi, J. Li-Modified Metal-Organic Frameworks for CO_2/CH_4 Separation: a Route to Achieving High Adsorption Selectivity. *J Mater. Chem.* **2010**, *20*, 706−714.
(89) Babarao, R.; Jiang, J.; Sandler, S. I. Molecular Simulations for Adsorptive Separation of CO_2/CH_4 Mixture in Metal-Exposed, Catenated, and Charged Metal-Organic Frameworks. *Langmuir* **2009**, *25*, 5239−5247.

(90) Huang, H.; Zhang, W.; Liu, D.; Zhong, C. Understanding the Effect of Trace Amount of Water on CO_2 Capture in Natural Gas Upgrading in Metal-Organic Frameworks: A Molecular Simulation Study. *Ind. Eng. Chem. Res.* **2012**, *51*, 10031−10038.
(91) Herm, Z. R.; Krishna, R.; Long, J. R. Reprint of: CO_2/CH_4, CH_4/H_2 and $CO_2/CH_4/H_2$ Separations at High Pressures Using Mg_2(dobdc). *Microporous Mesoporous Mater.* **2012**, *157*, 94−100.
(92) Hong, D. H.; Suh, M. P. Selective CO_2 Adsorption in a Metal-Organic Framework Constructed from an Organic Ligand with Flexible Joints. *Chem. Commun.* **2012**, *48*, 9168−9170.
(93) Spek, A. Single-Crystal Structure Validation with the Program PLATON. *J. Appl. Crystallogr.* **2003**, *36*, 7−13.